

Qubit-compatible substrates with superconducting through-silicon vias

K. GRIGORAS¹, N. YURTTAGÜL¹, J.-P. KAIKKONEN¹, E. T. MANNILA¹, P. ESKELINEN¹, D. P. LOZANO², H.-X. LI², M. ROMMEL², D. SHIRI², N. TIENCKEN¹, S. SIMBIEROWICZ¹, A. RONZANI¹, J. HÄTINEN¹, D. DATTA¹, V. VESTERINEN¹, L. GRÖNBERG¹, J. BIZNÁROVÁ², A. FADAVI ROUDSARI², S. KOSEN², A. OSMAN², J. HASSEL¹, J. BYLANDER², J. GOVENIUS¹,

¹VTT Technical Research Centre of Finland Ltd., QTF Centre of Excellence, P.O. Box 1000, FI-02044 VTT Espoo, Finland

²Department of Microtechnology and Nanoscience, Chalmers University of Technology, 412 96 Gothenburg, Sweden

Corresponding author: E. T. Mannila (email: elsa.mannila@vtt.fi).

arXiv:2201.10425v1 [quant-ph] 25 Jan 2022

ABSTRACT We fabricate and characterize superconducting through-silicon vias and electrodes suitable for superconducting quantum processors. We measure internal quality factors of a million for test resonators excited at single-photon levels, when vias are used to stitch ground planes on the front and back sides of the wafer. This resonator performance is on par with the state of the art for silicon-based planar solutions, despite the presence of vias. Via stitching of ground planes is an important enabling technology for increasing the physical size of quantum processor chips, and is a first step toward more complex quantum devices with three-dimensional integration.

I. INTRODUCTION

CORE performance metrics of superconducting qubits have rapidly improved since their inception, with dephasing time in particular increasing four orders of magnitude from 20 nanoseconds demonstrated by Chiorescu et al. [1] to hundreds of microseconds demonstrated recently [2]–[5]. To an extent, this astonishing progress in coherence time has been achieved by avoiding complexity in fabrication. State-of-the-art superconducting qubits are typically fabricated using an extremely restricted set of materials, a low thermal budget, and a small number of depositions and lithographies, often including techniques such as lift-off that are problematic for high yield in large devices.

Besides long coherence times required to achieve high fidelity of the fundamental single and two-qubit gates, quantum computers also need to become large to solve useful computing tasks. For example, tens or hundreds of millions of physical qubits are likely required for factoring thousand-bit numbers using Shor’s algorithm, due to overhead associated with error correction [6]. Coherent operations can fortunately be restricted to nearest neighbors in the surface code [7], which is currently the most promising approach to error correction. The two-dimensional nature of nearest-neighbor coupling makes a physical implementation of a large quantum computer more feasible, but separate control and readout lines still need to address essentially all of the qubits. Routing the control and readout lines around coherent couplers therefore necessitates the use of more than a single

electrode layer in larger quantum processors. Consequently, moving to more complex fabrication seems unavoidable, either monolithically or by using multichip modules. Flip-chip bonded modules of two chips connected by superconducting bumps increase the layer count to two and air bridges further alleviate routing challenges. These have indeed been used successfully to construct processors of several dozen qubits [8]–[10], although with coherence times and gate fidelities significantly lower than in planar [11]–[15] or flip-chip bonded [16] single- or few-qubit devices.

Superconducting vias compatible with high-coherence qubits are an important next step toward larger processors. In addition to routing purposes, so called via stitching is likely needed to shunt nominally grounded planes in different layers, in order to control and push up the frequencies of harmful parasitic microwave modes that become problematic in physically large processors [17]. Traditional integrated circuit vias are, however, optimized for different goals, such as high normal-state conductivity and reduction of parasitic capacitance, instead of superconductivity and extremely low microwave loss required for qubit compatibility. Integrating their fabrication with qubits also poses challenges related to material compatibilities and the low thermal budget of aluminum-based qubits. Superconducting vias have long been used for multilayer wiring in superconducting quantum interference (SQUID) and single-flux quantum (SFQ) devices [18], [19], but the vias are shallow and pass through amorphous dielectric layers with poor microwave perfor-

mance.

Yost *et al.* [20], [21] have on the other hand demonstrated through-silicon vias (TSVs) that have relatively high aspect ratio, high critical current, and show promise in terms of not destroying qubit coherence, as the demonstrated qubit relaxation time of $12.5 \mu\text{s}$ [20] and resonator internal quality factors of 10^5 to 2×10^5 [21] were identified to be limited by factors unrelated to TSVs. Widely-reproduced relaxation times for transmon qubits on silicon substrates are near $50 \mu\text{s}$ [11]–[16]. In addition, Gordon *et al.* have reported relaxation times of hundreds of μs [4]. Corresponding reproducible resonator quality factors are roughly one million for typical coplanar waveguide (CPW) test resonator geometries [12], [13], [22]–[24], although this can be exceeded with deep trenching or short-lived oxide removal treatments [25]–[27]. Resonator quality factor is often used as a diagnostic predictor of qubit relaxation time for a qubit with electrodes fabricated using the same flow as the resonators. Others have also fabricated superconducting TSVs but microwave performance of those approaches remains to be measured [28]–[30]. Furthermore, coherence times exceeding $300 \mu\text{s}$ have recently been demonstrated for transmon qubits on planar sapphire substrates [2], [3]. Typical methods of etching TSVs using the Bosch process are, however, not applicable to sapphire substrates.

In this article, we report on resonator internal quality factors of roughly a million measured on chips with TSVs stitching the ground planes on the front and back. The TSVs and resonators are fabricated on full 150 mm wafers, with a via-last approach where the first electrode layer is deposited and patterned before via formation. The via-last approach ensures a high-quality interface between the substrate and the critical electrode layer used for the resonators. Furthermore, the tantalum-based electrode layer used here has relatively low kinetic inductance similar to commonly used niobium films. While high kinetic inductance is useful in superinductors, for example in the fluxonium shunt inductor [31], kinetic inductance in electrodes of transmon qubits is not typically desirable. Low kinetic inductance tends to also yield better parameter control since geometric inductance is often more accurately reproducible than kinetic inductance.

II. DEVICE STRUCTURE

Fig. 1 presents our TSV structure consisting of the main electrode layer on the front side of the wafer, a hollow via with metallized walls, a metal membrane covering the via on the front side of the wafer, and a metallized back side (not visible). The electrode layer on the front side consists of a bilayer of 15 nm of titanium nitride and 200 nm of tantalum sputtered on high-resistivity silicon. For brevity, we refer to this as the tantalum-based electrode layer. The inner walls of the vias and the back side of the wafer are coated with nominally 280 nm of titanium nitride using plasma-enhanced atomic layer deposition (ALD). The membrane covering each via on the front side of the wafer consists of 2 μm of sputtered titanium nitride. The membranes survive typical wafer level handling and processing, although most of them

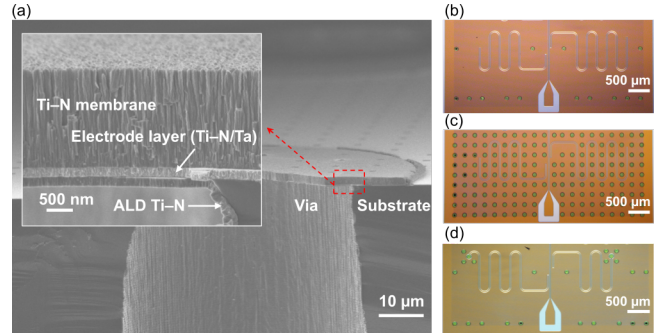


FIGURE 1. (a) Scanning electron microscope images of a TSV. (b,c,d) Optical micrographs showing layouts with different densities and roles of TSVs (green circles): (b) sparse via stitching, (c) dense via stitching, (d) TSV-terminated resonators.

cleave off during the final dicing step. This is not a significant issue for the resonator samples characterized here but the fragility of the membranes may be an inconvenience in some applications requiring post processing on diced chips.

The aspect ratio of our TSVs is approximately eight, with a nominal TSV diameter of $60 \mu\text{m}$ and substrate thickness of $525 \mu\text{m}$. The aspect ratio is similar to that of Refs. [20], [21], although we have not concentrated on maximizing it. It should be possible to increase the aspect ratio in the future since the only coating needed inside the vias is produced by ALD, which is highly conformal. Furthermore, smaller via diameter is likely achievable with thinner wafers, even without increasing aspect ratio. This would increase density as well as the mechanical robustness of the metal membranes covering the vias.

The main results reported in this article are measured from CPW resonators patterned on chips with TSVs as well as planar reference chips, fabricated from Nb or from the same Ta-based electrode layer as the TSV chips. The TSV chips have two to eight CPW resonators coupled to a common feedline through which transmission is measured (see Fig. 1). Each resonator acts as a bandstop filter at each of its resonance frequencies, and thus provides a sensitive probe of microwave loss at those frequencies, assuming the internal quality factor Q_i and coupling quality factor Q_c are of similar order of magnitude. Here, the resonators are open near the feedline and shorted at the opposite end, with geometry chosen such that the fundamental $\lambda/4$ resonance frequency varies between 4 and 8 GHz and the coupling quality factor between 2×10^4 and 7×10^6 . The width of the CPW center trace is $20 \mu\text{m}$ and the gap between the center and ground is $10 \mu\text{m}$, as in Ref. [24]. Overetching past the metal layer is small, less than roughly 50 nm , and no additional trenching is applied. The exact dimensions of the CPW cross section are significant when making direct quantitative comparisons since in low-loss resonators, the losses are generally dominated by material imperfections in thin interface layers between different materials, and the participation factors of different interfaces are somewhat geometry dependent [32]–[35].

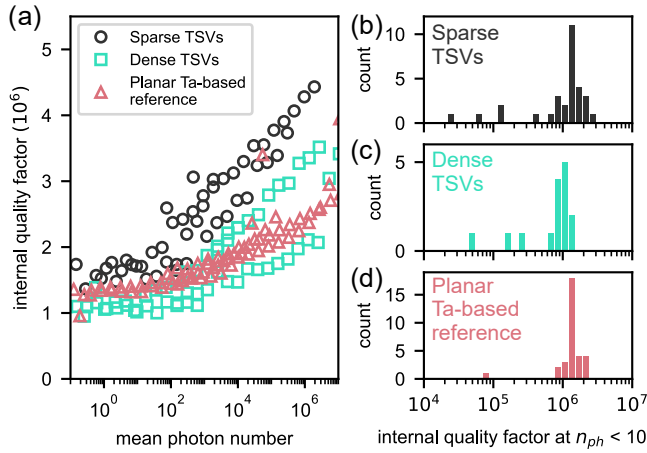


FIGURE 2. Quality factor measurements for via stitched TSV chips: (a) Measured internal quality factors Q_i at 10 mK as a function of photon number n_{ph} circulating in resonator for resonators with sparse stitch TSVs (circles), dense stitch TSVs (squares), and planar reference resonators with the same Ta-based electrode layer (red). For clarity, data are shown for only two resonators with frequency between 4 GHz and 5.5 GHz for each device type. (b,c,d) Histogram of measured internal quality factors at low photon numbers for all measured resonators of the types shown in panel (a).

In terms of density and role of TSVs, we use four types of layouts on the measured devices: (a) no TSVs and no ground plane on the back used as reference, (b) sparse TSVs stitching the ground planes on the front and back, (c) dense TSVs stitching the ground planes, and (d) sparse TSVs stitching the grounds and TSVs terminating the resonators to the ground on the back. As shown in Fig. 1, the sparse TSV design (b) has a spacing of 0.5 to 2 mm between the TSVs in areas near the resonators, with each resonator having one to three stitch vias at a distance of 150 to 300 μm from the center trace. This design aims to minimize the currents and electric fields induced in the vias when the resonators are excited, while still providing sufficiently dense via stitching for the ground planes to increase the frequency of the parasitic chip modes above the measurement band. The dense TSV design (c) greatly increases the participation of the stitch vias in the resonant modes by increasing their number and proximity to the center trace. The TSV-terminated design (d) makes the TSVs at the end of the resonator an integral part of the resonator, and has three or four stitch vias at a distance of 160 μm from each termination, in addition to the sparse stitch via pattern of design (b). The back ends of the terminating TSVs are approximately at a voltage node of the resonators, but the non-negligible physical and electrical length of the vias implies that the ends of the vias on the front side are roughly 0.02λ away from the voltage node.

III. QUALITY FACTOR MEASUREMENTS

Figure 2(a) shows that the best resonator chips with sparse TSVs stitching the front and back ground planes perform as well as the best planar reference samples with the same tantalum-based electrode layer. Furthermore, the resonator performance is similar to other reported results for silicon

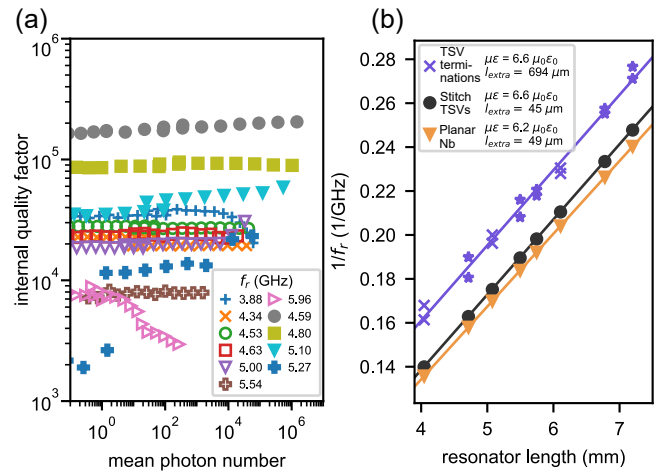


FIGURE 3. (a) Internal quality factor versus photon number for TSV-terminated resonators. Data points end at the right at relatively low powers due to poor fit of the model to asymmetric line shapes at high powers, and data is not shown for those resonances where $Q_i \ll Q_c$ leading to large uncertainty in fitting. (b) Inverse resonance frequencies of several chips with TSV-terminated resonators (purple crosses and stars), resonator with sparse via stitching (black circles), and reference Nb resonators (orange triangles) versus length of the coplanar part. Crosses (stars) indicate a TSV termination with three (four) ground vias around the terminating TSV. Solid lines indicate fits to Eq. (1) with parameters given in the legend.

substrates, and suggests that transmon-type qubits patterned on the same electrode layer could achieve state-of-the-art coherence. This is the main result reported in this article as it demonstrates that none of the processing steps required to form the TSVs is fundamentally detrimental to coherence. Even though the TSVs are not strongly coupled to the most sensitive long-coherence elements on the chip, via stitching of the ground planes compatible with high-coherence qubits is an important advancement in itself, as it allows physically larger quantum processor chips.

We draw this conclusion by comparing the best TSV chips to the best reference chips since certain uniformity and yield issues remain to be solved. This can be seen in the histogram in Fig. 2(b) showing a small fraction of outlier resonators with anomalously low quality factors, which are relatively power independent. We occasionally find such outliers also in planar reference devices. Furthermore, resonators near the edges of the 150 mm wafers show Q_i below 10^5 , even for the sparse TSV test design. In this article, we exclude the edge chips, as high throughput of the process has not yet been a development priority and we assume that uniformity of the processing steps can be improved in the future.

We observe somewhat decreased Q_i in chips with dense stitch vias [Fig. 2(a)]. In resonators terminated with TSVs, the internal quality factors are drastically lower, ranging from Q_i less than 10^4 to 2×10^5 , as shown in Fig. 3. The line shapes of TSV-terminated resonators generally become asymmetric at just 10^3 to 10^5 photons, after which the model used to extract Q_i [36] from the response no longer fits well. This threshold power is many orders of magnitude lower than for all resonators without TSV termination, for which we observe

such a threshold only above powers corresponding to over 10^7 photons. Furthermore, TSV-terminated resonators show essentially no power dependence of Q_i , until the nonlinearity leading to asymmetric response becomes significant.

These observations suggest that, unlike in the resonators with Q_i in the range of a million, two-level systems (TLSs) in thin dielectric interface layers are not a significant loss mechanism for the TSV-terminated resonators, as they would be expected to lead to quality factors increasing with photon number. It is instead possible that the ALD titanium nitride film on the inner walls of the hollow TSVs contains weak spots with suppressed superconductivity. This should lead to rapid decrease of quality factor at powers where the current through the termination becomes comparable to the critical current of the weak spot. DC characterization of critical currents (Fig. 5) indeed suggests that the critical current is as low as tens of μA for many of the vias. The best resonators perform as well as the TSV-interrupted resonators in Ref. [21], and the large variation we observe in Q_i could be related to the large range of critical currents and normal-state resistances measured even in adjacent vias [Fig. 5(c)].

On a positive note, the resonance frequencies f_r of the TSV-terminated resonators are consistent with those of other resonators, with approximately $650 \mu\text{m}$ of CPW-equivalent length added by the TSV termination, consistent with a wafer thickness of $525 \mu\text{m}$. In Fig. 3(b) we show inverse resonance frequencies versus the resonator length l_{design} for different resonator types as well as fits to

$$1/f_r = 4\sqrt{\mu\epsilon}(l_{design} + l_{extra}), \quad (1)$$

where the speed of light in the CPW $1/\sqrt{\mu\epsilon}$ and extra CPW-equivalent length l_{extra} are fit parameters. However, the deviation of the measured resonance frequencies from the frequencies predicted by the linear fit is relatively large for TSV-terminated resonators, showing an average deviation of 2% even within a single chip, as compared to less than 0.05% in references with no TSVs or stitch vias only. The variation in the resonance frequencies from the prediction of the linear fit is not explained by the different termination designs (three or four grounding TSVs surrounding the via terminating the resonator, see Fig. 1(d)). For resonators without TSV terminations, Fig. 3(b) shows no significant difference in the resonance frequencies between resonators with stitch vias and those patterned on a reference Nb film, demonstrating low kinetic inductance of the tantalum-based electrode layer and therefore high compatibility with existing designs.

Although the performance of the TSV-terminated resonators is modest, the loss is likely negligible in transmission line applications without resonators. If additional backside processing is added, the TSVs are likely suitable for integration in charge excitation and qubit readout lines where attenuation at the level of $1/10^4$ per TSV is negligible and sub- μA currents are typically sufficient.

Fig. 4 shows comparisons of the sparse TSV results with planar reference resonators made out of niobium, with panel (a) showing the power dependence for a few exemplary

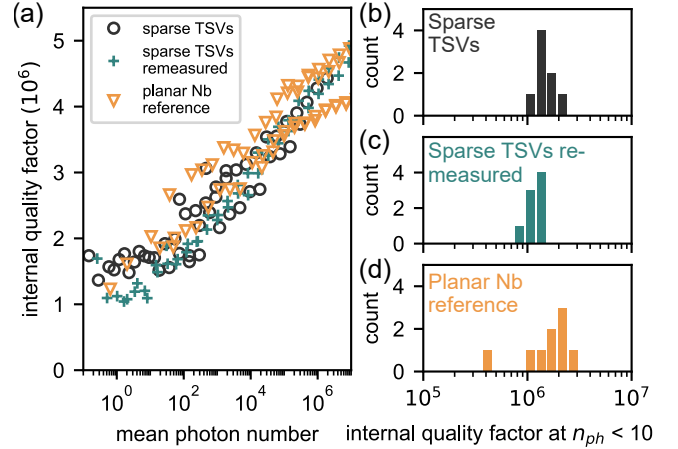


FIGURE 4. (a) Internal quality factor versus photon number for sparse TSV resonators (black circles) compared to reference measurements: the same device measured two weeks later (stars), as well as conventional planar Nb resonators (triangles). For clarity, only two resonances are shown per device. (b,c,d) Histograms of low-power Q_i for the chips shown in panel (a).

resonators and panels (b,c,d) showing the low-power Q_i for all resonators on the chips. At single-photon powers, the resonators with sparse stitch vias perform approximately identically to the niobium reference. Figure 4 also shows that the results measured on a chip with sparse TSV stitching do not change much when the chip is left at room temperature and atmospheric pressure for two weeks between measurements. This is consistent with our observation (not shown) that planar reference samples with the same tantalum-based electrode layer are also stable in time. The data for all resonator types in Fig. 4(a) are qualitatively similar, and the dependence of Q_i on photon number is relatively weak. Finally, we obtain an estimate for the total TLS loss $F\delta_{TLS}^0$ as $F\delta_{TLS}^0 = \delta_{LP} - \delta_{HP}$, where $\delta_{LP}(\delta_{HP})$ is the loss calculated as $1/Q_i$ at low (high) power. The obtained value $F\delta_{TLS}^0 \simeq 5 \times 10^{-7}$ is of the same order of magnitude as best reported results for planar devices [22], although the relatively weak power dependence makes this estimate rather rough.

IV. DC CHARACTERIZATION

The superconducting transition temperature of the tantalum-based electrode layer is slightly above 4 K [Fig. 5(a)], in line with a literature value of 4.46 K for high-purity bulk tantalum [37]. On the planar back side of the wafer, the ALD titanium nitride coating has a transition temperature in excess of approximately 2 K, which is typical for highly disordered titanium nitride deposited by ALD. The critical temperature is significantly below highest values achieved with ALD or other methods (4.5 to 5.4 K) [38] but easily satisfies the basic requirement of effectively suppressing thermal quasiparticles in superconducting qubit applications, which operate around 10 mK to 30 mK. The critical temperatures of the films were measured with standard lock-in techniques in a four-probe configuration.

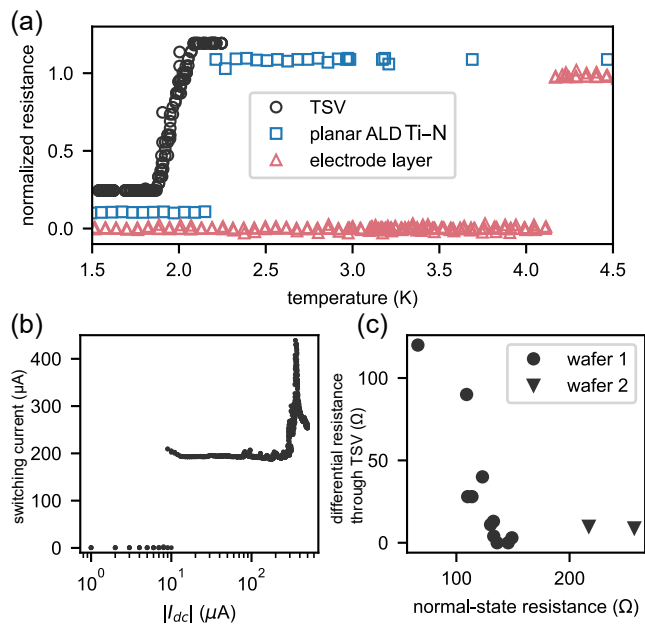


FIGURE 5. (a) Temperature dependence of normalized resistance for ALD titanium nitride inside a single via (circles), planar ALD titanium nitride (squares), and the planar tantalum-based electrode layer (triangles). For clarity, the traces are offset vertically by 0.1. (b) Differential resistance versus the absolute value of bias current I_{dc} through a single TSV at 100 mK, showing several switching currents. The response is symmetric around $I_{bias} = 0$. (c) Smallest switching current versus normal-state resistance for several different TSVs on two wafers.

The transition to the superconducting state is significantly broadened toward lower temperatures when measured through a single TSV, as also shown in Fig. 5(a). This is qualitatively similar to the broad transition observed by Mallek *et al.* [21]. Furthermore, Fig. 5(b) shows that the via switches from the superconducting state to the normal state gradually, in multiple steps from tens to hundreds of μ A, and the lowest switching current varies from a few microamperes to over 100 μ A [Fig. 5(c)]. Both of these observations are consistent with the existence of weak spots in the titanium nitride lining inside the via. The weakest spot determines the lowest switching current and, due to Joule heating, also likely limits the highest observed switching currents to only hundreds of μ A, which correspond to only a few kA/cm^2 of nominal current density.

V. CONCLUSIONS

In conclusion, we successfully fabricated and characterized qubit-compatible microwave resonators on silicon wafers with TSVs stitching the front and back ground planes. The resonator performance improves over previous results [21] by nearly an order of magnitude and is on par with fully planar resonator results, despite the added complexity of fabrication. The resonator performance provides strong evidence that state-of-the-art qubit coherence times would likely be reached if the same process were used for transmon-type qubits, with Josephson junctions post-processed on the samples using established evaporation-based methods. Stitching

the ground planes with TSVs is an important technique for controlling parasitic microwave modes within the silicon chip. Without TSVs or other methods for controlling them, the parasitic modes limit the physical size of transmon-based quantum processor chips to the range of a few dozen millimeters. Qubits fabricated on sapphire substrates have shown even better performance but there is no clear path to fabricating qubit-compatible high-aspect-ratio vias on sapphire substrates.

Critical currents of the TSVs demonstrated here leave room for future improvement. The low switching currents in dc measurements, decaying microwave performance at modest excitation powers, the existence of outliers in the microwave measurements, and the dramatically lower performance of via-terminated samples all hint in the direction of weak spots in the titanium nitride film inside the vias. This may be due to roughness of the via walls or due to imperfect conformality of the plasma-enhanced ALD process, which could lead to different film quality and weaker superconductivity at the far end of the via. Both of these potential issues can be improved incrementally without drastic changes to the TSV structure. Other possible future improvements include increasing the aspect ratio of the vias or reducing the thickness of the wafers, which would both lead to smaller diameter vias. Smaller diameter vias increase integration density and would improve the mechanical stability of the membranes covering the TSVs.

AUTHOR CONTRIBUTIONS

K. Grigoras led process development of via etching and ALD and was a key contributor to electrode and membrane layer development. N. Yurttagül and J.-P. Kaikkonen led process development of the electrode and membrane layers. E. T. Mannila led characterization and analysis efforts together with N. Tiencken. P. Eskelinen led process development of the final ALD recipe. A. Ronzani, J. Hättinen and S. Simbierowicz contributed to dc characterization throughout the process development. S. Simbierowicz also contributed to mask design. L. Grönberg, V. Vesterinen and S. Simbierowicz contributed to development of relevant planar resonators. D. Datta and V. Vesterinen contributed to rf measurements. D. P. Lozano did process development of electrode layer deposition and device characterization at Chalmers, used in earlier iterations of the devices that the reported devices improve upon. H.-X. Li contributed to device characterization. M. Rommel contributed to process development. D. Shiri contributed to microwave design and analysis. J. Biznárová, A. Fadavi Roudsari, S. Kosen, and A. Osman assisted in fabrication, characterization, and discussions. J. Bylander supervised the work at Chalmers. J. Govenius supervised and contributed technical advice to all aspects of the work, after a first phase supervised by J. Hassel.

ACKNOWLEDGMENT

This work was financially supported by OpenSuperQ, which has received funding from the European Union's Horizon

2020 research and innovation programme under grant agreement No 820363. The work at VTT was supported by the Quantum Computer Codevelopment project funded by the Finnish government, and performed as part of the Academy of Finland Centre of Excellence program (projects 336817, 312059 and 312294). The Chalmers work was in part supported by the Wallenberg Center for Quantum Technology, and performed at Myfab Chalmers.

REFERENCES

- [1] I. Chiorescu, Y. Nakamura, C. J. P. M. Harmans, and J. E. Mooij, "Coherent Quantum Dynamics of a Superconducting Flux Qubit," *Science*, vol. 299, no. 5614, pp. 1869–1871, 2003.
- [2] A. P. M. Place, L. V. H. Rodgers, P. Mundada, B. M. Smitham, M. Fitzpatrick, Z. Leng, A. Premkumar, J. Bryon, A. Vrajitoarea, S. Sussman, G. Cheng, T. Madhavan, H. K. Babla, X. H. Le, Y. Gang, B. Jäck, A. Gyenis, N. Yao, R. J. Cava, N. P. de Leon, and A. A. Houck, "New material platform for superconducting transmon qubits with coherence times exceeding 0.3 milliseconds," *Nat Commun*, vol. 12, no. 1, p. 1779, Dec. 2021. [Online]. Available: <http://www.nature.com/articles/s41467-021-22030-5>
- [3] C. Wang, X. Li, H. Xu, Z. Li, J. Wang, Z. Yang, Z. Mi, X. Liang, T. Su, C. Yang et al., "Towards practical quantum computers: transmon qubit with a lifetime approaching 0.5 milliseconds," *npj Quantum Information*, vol. 8, no. 3, 2022.
- [4] R. Gordon, C. Murray, C. Kurter, M. Sandberg, S. Hall, K. Balakrishnan, R. Shelby, B. Wacaser, A. Stabile, J. Sleight et al., "Environmental radiation impact on lifetimes and quasiparticle tunneling rates of fixed-frequency transmon qubits," *arXiv preprint arXiv:2105.14003*, 2021.
- [5] A. Somoroff, Q. Ficheux, R. A. Mencia, H. Xiong, R. V. Kuzmin, and V. E. Manucharyan, "Millisecond coherence in a superconducting qubit," *arXiv preprint arXiv:2103.08578*, 2021.
- [6] A. G. Fowler, M. Mariantoni, J. M. Martinis, and A. N. Cleland, "Surface codes: Towards practical large-scale quantum computation," *Physical Review A*, vol. 86, no. 3, p. 032324, Sep. 2012. [Online]. Available: <https://link.aps.org/doi/10.1103/PhysRevA.86.032324>
- [7] S. B. Bravyi and A. Y. Kitaev, "Quantum codes on a lattice with boundary," *arXiv:quant-ph/9811052*, Nov. 1998, *arXiv: quant-ph/9811052*. [Online]. Available: <http://arxiv.org/abs/quant-ph/9811052>
- [8] F. Arute, K. Arya, R. Babbush, D. Bacon, J. C. Bardin, R. Barends, R. Biswas, S. Boixo, F. G. S. L. Brandao, D. A. Buell, B. Burkett, Y. Chen, Z. Chen, B. Chiaro, R. Collins, W. Courtney, A. Dunsworth, E. Farhi, B. Foxen, A. Fowler, C. Gidney, M. Giustina, R. Graff, K. Guerin, S. Habegger, M. P. Harrigan, M. J. Hartmann, A. Ho, M. Hoffmann, T. Huang, T. S. Humble, S. V. Isakov, E. Jeffrey, Z. Jiang, D. Kafri, K. Kechedzhi, J. Kelly, P. V. Klimov, S. Knysh, A. Korotkov, F. Kostritsa, D. Landhuis, M. Lindmark, E. Lucero, D. Lyakh, S. Mandrà, J. R. McClean, M. McEwen, A. Megrant, X. Mi, K. Michielsen, M. Mohseni, J. Mutus, O. Naaman, M. Neeley, C. Neill, M. Y. Niu, E. Ostby, A. Petukhov, J. C. Platt, C. Quintana, E. G. Rieffel, P. Roushan, N. C. Rubin, D. Sank, K. J. Satzinger, V. Smelyanskiy, K. J. Sung, M. D. Trevithick, A. Vainsencher, B. Villalonga, T. White, Z. J. Yao, P. Yeh, A. Zalcman, H. Neven, and J. M. Martinis, "Quantum supremacy using a programmable superconducting processor," *Nature*, vol. 574, no. 7779, pp. 505–510, Oct. 2019. [Online]. Available: <http://www.nature.com/articles/s41586-019-1666-5>
- [9] Y. Wu, W.-S. Bao, S. Cao, F. Chen, M.-C. Chen, X. Chen, T.-H. Chung, H. Deng, Y. Du, D. Fan, M. Gong, C. Guo, C. Guo, S. Guo, L. Han, L. Hong, H.-L. Huang, Y.-H. Huo, L. Li, N. Li, S. Li, Y. Li, F. Liang, C. Lin, J. Lin, H. Qian, D. Qiao, H. Rong, H. Su, L. Sun, L. Wang, S. Wang, D. Wu, Y. Xu, K. Yan, W. Yang, Y. Yang, Y. Ye, J. Yin, C. Ying, J. Yu, C. Zha, C. Zhang, H. Zhang, K. Zhang, Y. Zhang, H. Zhao, Y. Zhao, L. Zhou, Q. Zhu, C.-Y. Lu, C.-Z. Peng, X. Zhu, and J.-W. Pan, "Strong quantum computational advantage using a superconducting quantum processor," *Phys. Rev. Lett.*, vol. 127, p. 180501, Oct. 2021. [Online]. Available: <https://link.aps.org/doi/10.1103/PhysRevLett.127.180501>
- [10] P. Jurcevic, A. Javadi-Abhari, L. S. Bishop, I. Lauer, and D. F. Bogorin, M. Brink, L. Capelluto, O. Günliük, T. Itoko, N. Kanazawa et al., "Demonstration of quantum volume 64 on a superconducting quantum computing system," *Quantum Science and Technology*, vol. 6, no. 2, p. 025020, 2021.
- [11] J. M. Gambetta, C. E. Murray, Y.-K.-K. Fung, D. T. McClure, O. Dial, W. Shanks, J. W. Sleight, and M. Steffen, "Investigating Surface Loss Effects in Superconducting Transmon Qubits," *IEEE Trans. Appl. Supercond.*, vol. 27, no. 1, pp. 1–5, Jan. 2017. [Online]. Available: <http://ieeexplore.ieee.org/document/7745914/>
- [12] A. Dunsworth, A. Megrant, C. Quintana, Z. Chen, R. Barends, B. Burkett, B. Foxen, Y. Chen, B. Chiaro, A. Fowler, R. Graff, E. Jeffrey, J. Kelly, E. Lucero, J. Y. Mutus, M. Neeley, C. Neill, P. Roushan, D. Sank, A. Vainsencher, J. Wenner, T. C. White, and J. M. Martinis, "Characterization and reduction of capacitive loss induced by sub-micron {Josephson} junction fabrication in superconducting qubits," *Applied Physics Letters*, vol. 111, no. 2, p. 22601, 2017.
- [13] A. Nersisyan, S. Poletto, N. Alidoust, R. Manenti, R. Renzas, C.-V. Bui, K. Vu, T. Whyland, Y. Mohan, E. A. Sete, S. Stanwyck, A. Bestwick, and M. Reagor, "Manufacturing low dissipation superconducting quantum processors," *arXiv:1901.08042 [physics, physics:quant-ph]*, Jan. 2019, *arXiv: 1901.08042*. [Online]. Available: <http://arxiv.org/abs/1901.08042>
- [14] J. J. Burnett, A. Bengtsson, M. Scigliuzzo, D. Niepce, M. Kudra, P. Delsing, and J. Bylander, "Decoherence benchmarking of superconducting qubits," *npj Quantum Inf*, vol. 5, no. 1, p. 54, Dec. 2019. [Online]. Available: <http://www.nature.com/articles/s41534-019-0168-5>
- [15] A. Osman, J. Simon, A. Bengtsson, S. Kosen, P. Krantz, D. P. Lozano, M. Scigliuzzo, P. Delsing, J. Bylander, and A. Fadavi Roudsari, "Simplified Josephson-junction fabrication process for reproducibly high-performance superconducting qubits," *Appl. Phys. Lett.*, vol. 118, no. 6, p. 064002, Feb. 2021. [Online]. Available: <https://aip.scitation.org/doi/10.1063/5.0037093>
- [16] S. Kosen, H.-X. Li, M. Rommel, D. Shiri, C. Warren, L. Grönberg, J. Salonen, T. Abad, J. Biznárová, M. Caputo et al., "Building blocks of a flip-chip integrated superconducting quantum processor," *arXiv preprint arXiv:2112.02717*, 2021.
- [17] J. Wenner, M. Neeley, R. C. Bialczak, M. Lenander, E. Lucero, A. D. O'Connell, D. Sank, H. Wang, M. Weides, A. N. Cleland, and J. M. Martinis, "Wirebond crosstalk and cavity modes in large chip mounts for superconducting qubits," *Supercond. Sci. Technol.*, vol. 24, no. 6, p. 065001, Jun. 2011. [Online]. Available: <http://stacks.iop.org/0953-2048/24/i=6/a=065001?key=crossref.3720c132a3c926c0bcc3a171eab7ccce>
- [18] S. K. Tolpygo, V. Bolkhovskiy, T. Weir, L. M. Johnson, W. D. Oliver, and M. A. Gouker, "Deep sub-micron stud-via technology of superconductor vlsi circuits," *Superconductor Science and Technology*, vol. 27, no. 2, p. 025016, 2014.
- [19] M. Kiviranta, O. Brandel, L. Gronberg, J. Kunert, S. Linzen, N. Beev, T. May, and M. Prunnila, "Multilayer Fabrication Process for Josephson Junction Circuits Cross-Compatible Over Two Foundries," *IEEE Trans. Appl. Supercond.*, vol. 26, no. 6, pp. 1–5, Sep. 2016. [Online]. Available: <http://ieeexplore.ieee.org/document/7438771/>
- [20] D. R. W. Yost, M. E. Schwartz, J. Mallek, D. Rosenberg, C. Stull, J. L. Yoder, G. Calusine, M. Cook, R. Das, A. L. Day, E. B. Golden, D. K. Kim, A. Melville, B. M. Niedzielski, W. Woods, A. J. Kerman, and W. D. Oliver, "Solid-state qubits integrated with superconducting through-silicon vias," *npj Quantum Inf*, vol. 6, no. 1, p. 59, Dec. 2020. [Online]. Available: <http://www.nature.com/articles/s41534-020-00289-8>
- [21] J. L. Mallek, D.-R. W. Yost, D. Rosenberg, J. L. Yoder, G. Calusine, M. Cook, R. Das, A. Day, E. Golden, D. K. Kim, J. Knecht, B. M. Niedzielski, M. Schwartz, A. Sevi, C. Stull, W. Woods, A. J. Kerman, and W. D. Oliver, "Fabrication of superconducting through-silicon vias," *arXiv:2103.08536 [cond-mat, physics:physics, physics:quant-ph]*, Mar. 2021, *arXiv: 2103.08536*. [Online]. Available: <http://arxiv.org/abs/2103.08536>
- [22] C. R. H. McRae, H. Wang, J. Gao, M. R. Vissers, T. Brecht, A. Dunsworth, D. P. Pappas, and J. Mutus, "Materials loss measurements using superconducting microwave resonators," *Rev. Sci. Instrum.*, p. 23, 2020.
- [23] C. T. Earnest, J. H. Béjanin, T. G. McConkey, E. A. Peters, A. Korinek, H. Yuan, and M. Mariantoni, "Substrate surface engineering for high-quality silicon/aluminum superconducting resonators," *Supercond. Sci. Technol.*, vol. 31, no. 12, p. 125013, Dec. 2018. [Online]. Available: <http://stacks.iop.org/0953-2048/31/i=12/a=125013?key=crossref.480b00947cc57565899940f05b0c1539>
- [24] J. Burnett, A. Bengtsson, D. Niepce, and J. Bylander, "Noise and loss of superconducting aluminium resonators at single photon energies," *J. Phys.: Conf. Ser.*, vol. 969, p. 012131, Mar. 2018. [Online]. Available: <https://iopscience.iop.org/article/10.1088/1742-6596/969/1/012131>
- [25] G. Calusine, A. Melville, W. Woods, R. Das, C. Stull, V. Bolkhovskiy, D. Braje, D. Hover, D. K. Kim, X. Miloshi et al., "Analysis and mitiga-

- tion of interface losses in trenched superconducting coplanar waveguide resonators,” *Applied Physics Letters*, vol. 112, no. 6, p. 062601, 2018.
- [26] M. V. P. Altoé, A. Banerjee, C. Berk, A. Hajr, A. Schwartzberg, C. Song, M. A. Ghadeer, S. Aloni, M. J. Elowson, J. M. Kreikebaum, E. K. Wong, S. Griffin, S. Rao, A. Weber-Bargioni, A. M. Minor, D. I. Santiago, S. Cabrini, I. Siddiqi, and D. F. Ogletree, “Localization and reduction of superconducting quantum coherent circuit losses,” arXiv:2012.07604 [cond-mat, physics:quant-ph], Dec. 2020, arXiv: 2012.07604. [Online]. Available: <http://arxiv.org/abs/2012.07604>
- [27] J. Verjauw, A. Potočnik, M. Mongillo, R. Acharya, F. Mohiyaddin, G. Simion, A. Pacco, T. Ivanov, D. Wan, A. Vanleenhove, L. Souriau, J. Jussot, A. Thiam, J. Swerts, X. Piao, S. Couet, M. Heyns, B. Govoreanu, and I. Radu, “Investigation of Microwave Loss Induced by Oxide Regrowth in High- Q Niobium Resonators,” *Phys. Rev. Applied*, vol. 16, no. 1, p. 014018, Jul. 2021. [Online]. Available: <https://link.aps.org/doi/10.1103/PhysRevApplied.16.014018>
- [28] C. A. Jhabvala, D. J. Benford, R. P. Brekosky, M.-P. Chang, N. P. Costen, A. M. Datesman, G. C. Hilton, K. D. Irwin, A. J. Kogut, J. Lazear, E. S. Leong, S. F. Maher, T. M. Miller, S. H. Moseley, E. H. Sharp, J. G. Staguhn, and E. J. Wollack, “Kilopixel backshort-under-grid arrays for the Primordial Inflation Polarization Explorer,” in *Millimeter, Submillimeter, and Far-Infrared Detectors and Instrumentation for Astronomy VII*, W. S. Holland and J. Zmuidzinas, Eds., vol. 9153, International Society for Optics and Photonics. SPIE, 2014, pp. 1038 – 1048. [Online]. Available: <https://doi.org/10.1117/12.2056995>
- [29] M. Vahidpour, W. O’Brien, J. T. Whyland, J. Angeles, J. Marshall, D. Scarabelli, G. Crossman, K. Yadav, Y. Mohan, C. Bui, V. Rawat, R. Renzas, N. Vodrahalli, A. Bestwick, and C. Rigetti, “Superconducting Through-Silicon Vias for Quantum Integrated Circuits,” arXiv:1708.02226 [physics, physics:quant-ph], Aug. 2017, arXiv: 1708.02226. [Online]. Available: <http://arxiv.org/abs/1708.02226>
- [30] J. A. Alfaro-Barrantes, M. Mastrangeli, D. J. Thoen, S. Visser, J. Bueno, J. J. A. Baselmans, and P. M. Sarro, “Highly-conformal sputtered through-silicon vias with sharp superconducting transition,” *Journal of Microelectromechanical Systems*, vol. 30, no. 2, pp. 253–261, 2021.
- [31] V. E. Manucharyan, J. Koch, L. I. Glazman, and M. H. Devoret, “Fluxonium: Single {Cooper-Pair} Circuit Free of Charge Offsets,” *Science*, vol. 326, no. 5949, pp. 113–116, 2009.
- [32] C. R. H. McRae, H. Wang, J. Gao, M. R. Vissers, T. Brecht, A. Dunsworth, D. P. Pappas, and J. Mutus, “Materials loss measurements using superconducting microwave resonators,” *Review of Scientific Instruments*, vol. 91, no. 9, p. 091101, Sep. 2020. [Online]. Available: <http://aip.scitation.org/doi/10.1063/5.0017378>
- [33] W. Woods, G. Calusine, A. Melville, A. Sevi, E. Golden, D. Kim, D. Rosenberg, J. Yoder, and W. Oliver, “Determining Interface Dielectric Losses in Superconducting Coplanar-Waveguide Resonators,” *Phys. Rev. Applied*, vol. 12, no. 1, p. 014012, Jul. 2019. [Online]. Available: <https://link.aps.org/doi/10.1103/PhysRevApplied.12.014012>
- [34] V. Lahtinen and M. Möttönen, “Effects of device geometry and material properties on dielectric losses in superconducting coplanar-waveguide resonators,” *J. Phys.: Condens. Matter*, vol. 32, no. 40, p. 405702, Sep. 2020. [Online]. Available: <https://iopscience.iop.org/article/10.1088/1361-648X/ab98c8>
- [35] D. Niepce, J. J. Burnett, M. G. Latorre, and J. Bylander, “Geometric scaling of two-level-system loss in superconducting resonators,” *Supercond. Sci. Technol.*, vol. 33, no. 2, p. 025013, Jan. 2020. [Online]. Available: <https://iopscience.iop.org/article/10.1088/1361-6668/ab6179>
- [36] S. Probst, F. Song, P. A. Bushev, A. V. Ustinov, and M. Weides, “Efficient and robust analysis of complex scattering data under noise in microwave resonators,” *Review of Scientific Instruments*, vol. 86, no. 2, p. 024706, 2015.
- [37] J. G. C. Milne, “Superconducting Transition Temperature of High-Purity Tantalum Metal,” *Phys. Rev.*, vol. 122, no. 2, pp. 387–388, Apr. 1961. [Online]. Available: <https://link.aps.org/doi/10.1103/PhysRev.122.387>
- [38] A. Torgovkin, S. Chaudhuri, A. Ruhtinas, M. Lahtinen, T. Sajavaara, and I. J. Maasilta, “High quality superconducting titanium nitride thin film growth using infrared pulsed laser deposition,” *Supercond. Sci. Technol.*, vol. 31, no. 5, p. 055017, May 2018. [Online]. Available: <https://iopscience.iop.org/article/10.1088/1361-6668/aab7d6>

• • •